Experimental Characterization of Idle Tones in Second-Order Bandpass ΣΔ Modulators

J.M. de la Rosa, B. Pérez-Verdú, F. Medeiro, R. del Río and A. Rodríguez-Vázquez

Instituto de Microelectrónica de Sevilla, IMSE (CNM-CSIC)
Edif. CNM-CICA, Avda. Reina Mercedes s/n, 41012 Sevilla, SPAIN
Phone: +34 95056666, FAX: +34 95056686, E-mail: jrosa@imse.cnm.es

Abstract

This paper analyses the tonal behaviour of the quantization noise in second-order bandpass ΣΔ modulators. The analysis performed for lowpass modulators is extended to the bandpass case. As a result, closed form expressions for the frequency of idle tones are derived for different cases regarding the signal center frequency position. All these results have been validated by measurements from a silicon prototype using fully differential switched-current circuits implemented in a standard 0.8μm CMOS technology(*).

1. Introduction

The development of *Bandpass* ΣΔ Modulators (BP-ΣΔMs) [1] was fundamentally motivated by their suitability to realize the A/D conversion of either Intermediate Frequency (IF) or Radio Frequency (RF) signals in modern digital radio receivers. The early A/D conversion permits to implement the IF stage in the digital side, thus allowing a digital control of the gain and the coefficients of the IF filter. This has numerous advantages as compared to the traditional (analog) radio receivers: reduction of interferences, programmability, etc...

A number of *switched-capacitor* (SC) CMOS BP-ΣΔM prototypes have been reported with different applications in digital radio communications [2]-[4]. However, the continuously reduction of devices geometries in VLSI CMOS technologies makes possible to integrate the IF and RF stages of a radio system onto a single chip. This fact has motivated the use of other analog techniques which are compatible with standard CMOS processes, such as *switched-current* (SI) [5], to implement BP-ΣΔMs [6].

Most of reported BP-ΣΔM ICs obtain their architecture by applying a $z^{-1} \rightarrow -z^{-2}$ transformation to a *Lowpass* ΣΔ Modulator (LP-ΣΔM). Because of this transformation, a Lth-order LP-ΣΔM becomes a $2L$th-order BP-ΣΔM, keeping most of the properties of the former. One of these properties is the presence of *idle* tones in the output spectrum of the modulator. This phenomenon is caused by the correlation between the input signal and the quantization error [7]. This non-linear behaviour of the quantization error is more significant as the number of internal levels of the quantizer and/or the order of the modulator decrease. Hence, the worst case corresponds to a 1st-order LP-ΣΔM with a 1-bit quantizer.

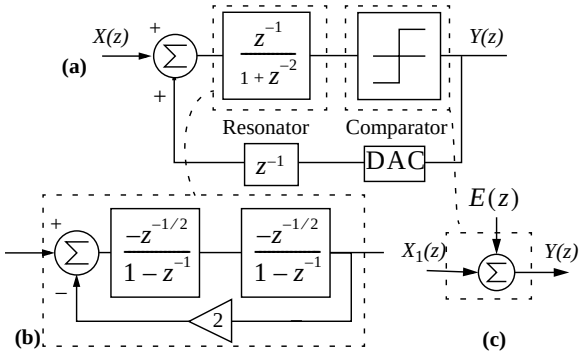

Fig. 1: (a) Block diagram of the modulator in this paper. (b) LDI-loop resonator. (c) Linear model of the quantizer.

The tonal behaviour of the quantization error in this class of ΣΔMs has been adequately analysed elsewhere [8][9][10]. However, very little has still been done for BP-ΣΔMs. Thus, the authors in [11] reported a non-linear analysis of a 2nd-order BP-ΣΔM for a sinusoidal input placed at a quarter of the sampling frequency (the ideal signal-band center frequency). However, as we demonstrated in [12], the signal band shifts as a consequence of circuit parasitics, and hence, this is a practical case which needs also to be analysed.

This paper demonstrates experimentally the correlation between the quantization error and the input signal in a 2nd-order BP-ΣΔM. The prototype, realized using fully differential regulated-folded cascode memory cells, was integrated in a 0.8μm standard CMOS technology. Measurements show that the results obtained for LP-ΣΔMs [8] can be extended to the bandpass case in order to explain the tonal behaviour of the quantization error in BP-ΣΔMs.

2. Ideal analysis of a 2nd-order BP-ΣΔM

Fig.1(a) shows the block diagram of a 2nd-order BP-ΣΔM. It has been obtained by applying a $z^{-1} \rightarrow -z^{-2}$ transformation to the 1st-order LP-ΣΔM of Fig.2. As a consequence of this transformation, the original integrator becomes a resonator. Thus, the first step towards the design of a BP-ΣΔM is choosing a suitable architecture to realize the resonator transfer

(*)This work has been supported by the Spanish CICYT Project TIC 97-0580.

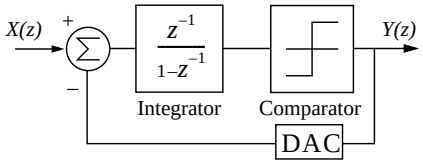

Fig. 2: Block diagram of a 1st-order LP-ΣΔM.

function. This can be realized using different topologies [3]. In this paper we will adopt a structure consisting of a feedback cascade of two *Lossless Discrete Integrators* (LDI), shown in Fig.1(b). This structure has been chosen because it keeps the poles inside the unit circle upon changes due to errors of the feedback loop gain. However, the use of this resonator requires an additional delay block to be included in the digital loop (see Fig.1(a)) in order to achieve the required delay in the modulator feedback loop.

A. Linear analysis

Assuming that the quantization error is modelled as an additive *white* noise source, the quantizer can be replaced by the linear model shown in Fig.1(c) [9][10]. In such a case, the modulator in Fig.1(a) can be viewed as a two-input, x and e, one output, y, system, which in the z-domain can be represented by

$$Y(z) = S_{\mathrm{TF}}(z)X(z) + N_{\mathrm{TF}}(z)E(z) \qquad (1)$$

where $S_{\mathrm{TF}}(z)$ and $N_{\mathrm{TF}}(z)$ represent the signal transfer function and the noise transfer function, respectively,

$$S_{\mathrm{TF}}(z) = z^{-1} \qquad N_{\mathrm{TF}}(z) = 1 + z^{-2} \qquad (2)$$

By making $z = \exp(j2\pi f/f_{\mathrm{s}})$, where f_{s} is the sampling frequency, it can be seen that $N_{\mathrm{TF}}(f)$ has one transmission zero at $f_{\mathrm{s}}/4$, and that the filtering around this frequency is actually of the band-stop type. The input signal is allowed to pass while, at the same time, most of the quantization noise power is "shaped" so that is pushed out of the signal band. This is illustrated in Fig.3 through an ideal simulated output spectrum for an input tone of –12dB input level†. Observe the presence of two *peaks* at both sides of the signal band. These peaks are due to the fact that the quantization error is not a white noise as has been assumed. This phenomenon will be discussed in the next section.

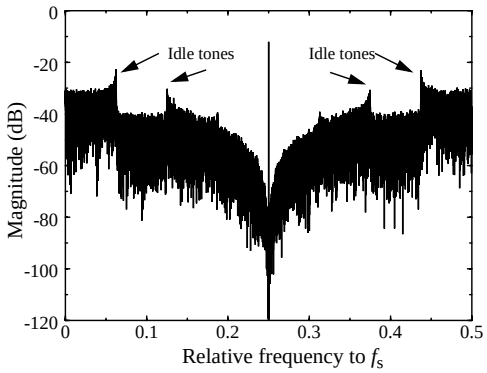

Fig. 3: Ideal modulator output spectrum.

The *in-band* quantization noise power can be calculated by integrating the output power spectral density within the signal bandwidth,

$$P_{\mathrm{Q}} = \int_{f_{\mathrm{s}}/4 - B_{\mathrm{w}}/2}^{f_{\mathrm{s}}/4 + B_{\mathrm{w}}/2} 2S_{\mathrm{Q}}\left|N_{\mathrm{TF}}(f)\right|^2 df \cong \frac{\Delta^2\pi^2}{36M^3} \qquad (3)$$

where $S_{\mathrm{Q}} = \Delta^2/(12f_{\mathrm{s}})$ is the power spectral density of the quantization noise, Δ is the quantization step, B_{w} is the signal bandwidth and $M \equiv f_{\mathrm{s}}/(2B_{\mathrm{w}})$ is the *oversampling ratio.* From (3), and assuming that the modulator input is a sinewave of amplitude $A \le \Delta/2$, the Signal-to-Noise Ratio (SNR) and the Dynamic Range (DR) are given by:

$$SNR = \frac{A^2}{2P_{\mathrm{Q}}} = \frac{18A^2M^3}{\pi^2\Delta^2} \qquad (4)$$

$$DR = \frac{(\Delta/2)^2}{2P_{\mathrm{Q}}} = \frac{9M^3}{2\pi^2} \qquad (5)$$

This shows that the modulator resolution increases with M at a rate of about 1.5-bit/octave. However, such an ideal feature can only be achieved provided that the scaling coefficients and the resonator transfer function in Fig.1(a) are realized without errors.

B. Non-linear analysis

In the linear model shown in Fig.1(c), the quantization error, $e \equiv y - x_1$, is assumed to be not correlated with the quantizer input, x_1. Actually, this error is a non-linear function of x_1, as illustrated in Fig.4 for an N-bit quantizer††.

If x_1 varies randomly from sample to sample in the interval $[x_{min}, x_{max}]$ (see Fig.4), e is largely uncorrelated with x_1 [7] and the linear model provides good results. This is achieved in LP-ΣΔMs for large modulator orders and $N > 1$ [10].

Hence, the worst case for applying the lineal model corresponds to a 1st-order modulator with a 1-bit quantizer like that in Fig.2. Candy [9] demonstrated that, for a dc input signal, the in-band quantization error power at the modulator output sharply changes with the input amplitude. This is illustrated in Fig.5(a) for $M = 64$ and $\Delta = 2$. This property of the

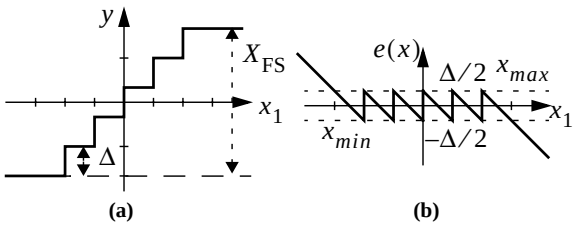

Fig. 4: Quantization process. (a) Ideal transfer characteristic. (b) Quantization error.

†. Input level is defined as the input signal referred to the DAC output level (= 0dB).

††. In the figure, X_{FS} stands for the full-scale range of the quantizer. Note that for $N = 1$, $X_{\mathrm{FS}} = \Delta$.

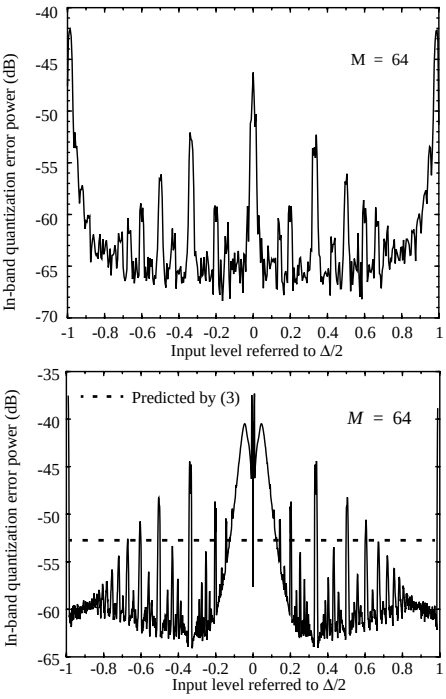

Fig. 5: Noise pattern for (a) a 1st-order LP-ΣΔM and (b) a 2nd-order BP-ΣΔM.

quantization error, often known as *noise pattern*, is translated to a 2nd-order BP-ΣΔM when the input signal is a single tone placed at $f_s/4$. This is illustrated in Fig.5(b) by showing the simulated in-band quantization error power at the output of Fig.1(a) as a function of the input amplitude. This behaviour can not be explained by the linear model (dashed line in Fig.5(b)) and hence, a non-linear analysis is required.

Gray [8] solved the non-linear difference equations of a 1st-order LP-ΣΔM. That analysis demonstrated that for dc inputs, the quantization error spectrum is discrete, with tones (often named *idle* tones) appearing at

$$f_{t_n} = \langle n\left(\frac{1}{2} \pm \frac{A_x}{\Delta}\right)\rangle f_s \qquad \text{for } n = 1, 2, \ldots \quad (6)$$

where A_x is the amplitude of x and $\langle a\rangle$ represents the fractional part of a. The amplitude of these tones is:

$$A_{t_n} = \frac{1}{(2\pi n)^2} \quad (7)$$

We can extend the above results to the bandpass case by simply applying the frequency translation $c \rightarrow f_s/4$ to (6). This obtains that the quantization error spectrum of a 2nd-order BP-ΣΔM with a sinusoidal signal placed at $f_s/4$ has pairs of idle tones at

$$f_{tbp_n} = f_s \begin{cases} \langle n\left(\frac{1}{4} \pm \frac{A_x}{2\Delta}\right)\rangle \\ \langle n\left(\frac{1}{2} \pm \frac{A_x}{2\Delta}\right)\rangle \end{cases} \qquad \text{for } n = 1, 2, \ldots \quad (8)$$

As an illustration, note that the most significant idle tones appearing in Fig.3 are located at $f_s/16$, $f_s/8$, $3f_s/8$ and $7f_s/16$. This corresponds to $A_x/\Delta = 1/8$ (–12dB input level) in (8).

3. Non-ideal analysis – effect of SI errors

In the previous section the modulator was assumed to be ideal except for the inherent quantization error. In practice, circuit parasitics will degrade the performance of the modulator.

Fig.6 shows a conceptual SI realization of the resonator in Fig.1(b) employing second generation SI memory cells. As shown in [5], the major error sources of SI memory cells are three, namely: *conductance error* (represented by parameter ε_g) due to finite input/output conductances; *incomplete settling error* (represented by ε_s), and *switch charge injection error* (represented by ε_q). Besides, the resonator behaviour becomes degraded by the finite conductances (g_{oF} and g_{oFB} in Fig.6) of the current mirrors employed to realize the scaling coefficients. Their associated errors are defined respectively by:

$$\begin{aligned} \varepsilon_F &= r_{on} g_{oF} & \varepsilon_{g_F} &= g_{oF}/g_{in} \\ \varepsilon_{FB} &= r_{on} g_{oFB} & \varepsilon_{g_{FB}} &= g_{oFB}/g_{in} \end{aligned} \quad (9)$$

where g_{in} is the input conductance of the memory cells and r_{on} is the on-resistance of the steering switches.

As we demonstrated in [12], the transfer function of the resonator degraded by SI errors is:

$$H_{res}^{e}(z) \cong \frac{(1-\mu_1)z^{-1}}{1 + \xi_1 z^{-1} + (1-\xi_2)z^{-2}} \quad (10)$$

where

$$\begin{aligned} \mu_1 &= 2\varepsilon_F + 2\varepsilon_s + 2\varepsilon_g + 2\varepsilon_q + \varepsilon_{g_F} \\ \xi_1 &= -(2\varepsilon_F + 2\varepsilon_{FB} + 4\varepsilon_s + \varepsilon_{g_F} + \varepsilon_{g_{FB}}) \\ \xi_2 &= 4\varepsilon_s + 4\varepsilon_g + 4\varepsilon_q + \varepsilon_{g_F} + \varepsilon_{g_{FB}} \end{aligned} \quad (11)$$

The above errors modify the noise transfer function N_{TF}. Thus, the zeroes of this function are shifted from their nominal positions – located at $f_s/4$ – degrading the noise shaping and making the in-band quantization noise power to increase.

Substituting (10) in the transfer function of the resonator in Fig.1(a), and following a similar procedure as in previous section, it can be shown that the dynamic range of a 2nd-order BP-ΣΔM in the presence of SI errors is given by:

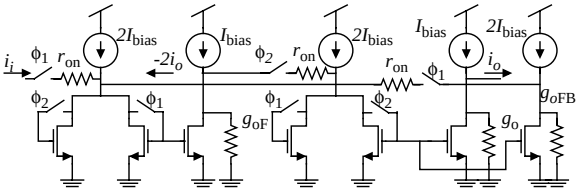

Fig. 6: Schematic of the resonator including SI Errors.

$$DR^{e} \cong \frac{9M^3}{2\pi^2\left[1+(3\xi_1^2+\xi_2^2)\left(\frac{M}{\pi}\right)^2\right]} \qquad (12)$$

Note that SI errors do not affect DR in the same way, the largest degradation being produced by ε_s.

In addition to the degradation on the dynamic range, SI errors cause the signal-band center frequency (often named *notch* frequency, f_n) to shift from its nominal position at $f_s/4$. As shown in [12], the error in f_n, denoted as δf_n, is approximately given by:

$$\delta f_n \equiv f_n - \frac{f_s}{4} \cong \xi_1 \frac{M}{\pi}\left(\frac{B_w}{2}\right) \qquad (13)$$

Note that, as $\xi_1 \le 0$ by definition, $f_n \le f_s/4$ for all SI BP-ΣΔMs.

Considering that the quantization noise power is minimum at f_n, the signal should be centered at f_n in order to obtain a maximum dynamic range. On the other hand, placing a single tone at a frequency different from $f_s/4$ in a BP-ΣΔM is equivalent to applying a sinusoidal signal of low frequency in a LP-ΣΔM. As demonstrated in [8], the output spectrum of a 1st-order LP-ΣΔM with a sinusoidal input signal of frequency, f_i, is discrete, having tones at

$$f_{t_n} = f_s \begin{cases} \langle n\frac{f_i}{f_s}\rangle \\ \langle n\frac{f_i}{f_s}-\frac{1}{2}\rangle \end{cases} \qquad \text{for } n = 1, 2, 3, \ldots \qquad (14)$$

We can extend this result for the bandpass case, by applying the frequency translation $c \to f_s/4$ to (14). This obtains that the output spectrum of a 2nd-order BP-ΣΔM will contain idle tones at

$$f_{tbp_n} = f_s \begin{cases} \langle\left(\frac{1}{4} \pm n\frac{\delta f_n}{2}\right)\rangle \\ \langle\left(\frac{1}{2} \pm n\frac{\delta f_n}{2}\right)\rangle \end{cases} \qquad \text{for } n = 1, 2\ldots \qquad (15)$$

Observe that, two families of tones appear at both sides of $f_s/4$ which can corrupt the signal information. This will be demonstrated by measurements in the next section.

4. Experimental results

The 2nd-order bandpass ΣΔ modulator of Fig.1(a) was realized using fully differential regulated-folded cascode memory cells. The 1-bit quantizer was made up of a regenerative latch and an RS flip-flop and the DAC consisted of a current source controlled by the comparator output.

Those building blocks were designed to attaining the requirements of direct A/D conversion in AM digital radio receivers, whose commercial broadcast band is from 540kHz to 1.6MHz with stations occupying a 10kHz wide band. This imposes that the sampling frequency must be tunable over the range f_s = 2MHz to f_s = 6.4MHz.

The circuit was fabricated in a CMOS 0.8μm double-metal single-poly technology. Fig. 7 shows the microphotograph of the chip. It also includes some isolate building blocks for testing separately. The active area of the modulator is 0.35mm^2 and the power consumption is 42mW from a 5V power supply.

For testing purposes, the modulator chip was attached to a two-layer PCB, which has been designed following the indications in [13]. The output bit streams were captured with the HP82000 data acquisition system. Kaiser(β = 20)-windowed 32768-point FFTs were performed on each of those bit streams using MATLAB [14].

A. Measurements for an input tone at $f_s/4$

Fig.8 shows several modulator output spectra when clocked at f_s = 2MHz. Note that, because of SI errors, the notch frequency is deviated from the ideal position (at $f_s/4$). In this case, $\xi_1 \cong 0.07$, which according to (13), yields f_n = 0.2455f_s.

As Fig.8 illustrates, there are four groups of idle tones whose frequencies are a function of the input signal amplitude. Note that, as A_x approaches to $\Delta/2$, two of these groups (labelled as L_1 and R_1 in Fig.8) move away from $f_s/4$ while the other two groups (L_2 and R_2) approach to $f_s/4$. The tones with the largest amplitude ($\cong$ –30dB) are those placed at:

$$\begin{aligned} f_{L1} &= \frac{f_s}{4}-\frac{A_x}{2\Delta}f_s & f_{R1} &= \frac{f_s}{4}+\frac{A_x}{2\Delta}f_s \\ f_{L2} &= \frac{A_x}{2\Delta}f_s & f_{R2} &= \frac{f_s}{2}-\frac{A_x}{2\Delta}f_s \end{aligned} \qquad (16)$$

which matches with that predicted by (8) for n = 1. As an illustration, Fig.9 represents f_{L1}, f_{L2}, f_{R1} and f_{R2} as a function of A_x/Δ, showing a good agreement between theory and measurements.

In AM radio applications, out-of-band idle tones are critical because, in the presence of non-linear errors, can mix with the input signal and fall into the signal band. For the special case of a single tone at $f_s/4$, the most significant intermodulation components (those corresponding to A_x approaching to Δ) will fall approximately at $f_s/4$, thus not degrading the linearity of the modulator. Fig.10 illustrates this by

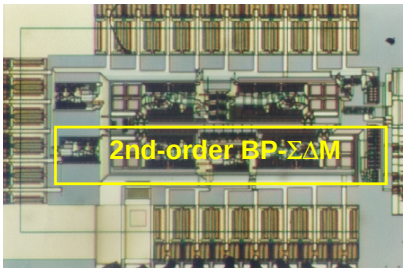

Fig. 7: Microphotograph of the modulator.

plotting the Signal-to-Noise + Distortion Ratio ($SNDR$) as a function of the input level for different sampling frequencies and $M = 128$. Note that a linear behaviour is obtained for all over the signal range.

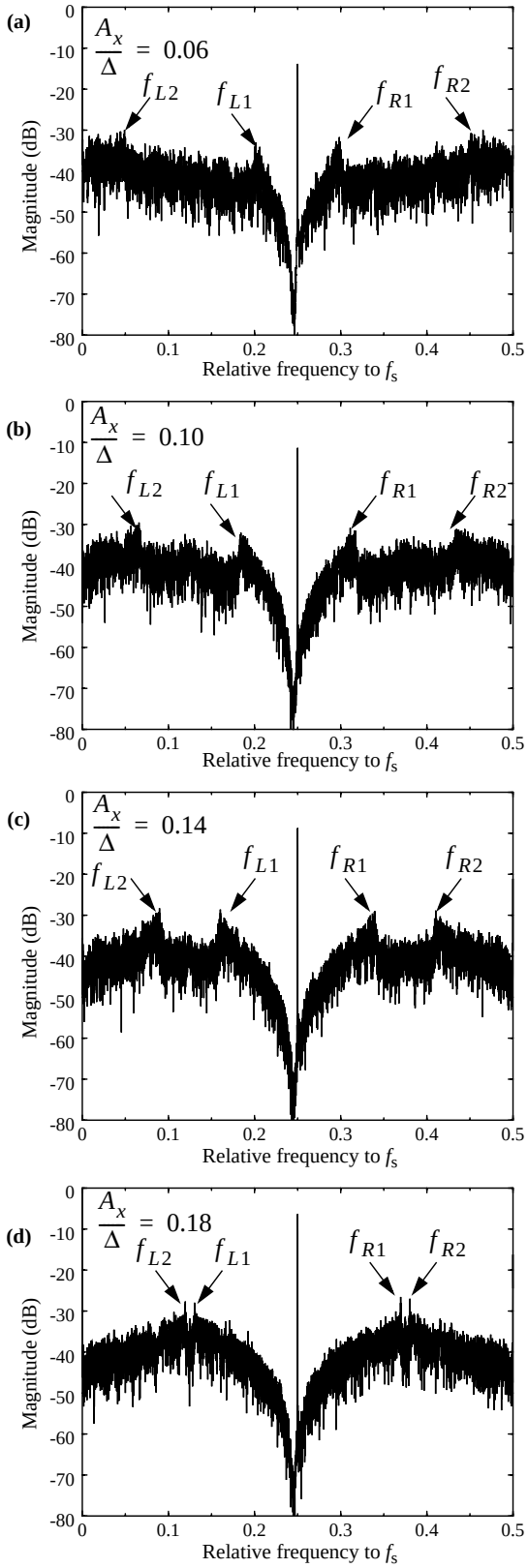

Fig. 8: Measured modulator output spectra when clocked at $f_s = 2\text{MHz}$ for an input tone of $f_s/4$ and different relative amplitudes: (a) -16.3dB, (b) -13.8dB, (c) -11.3dB, (d) -8.7dB.

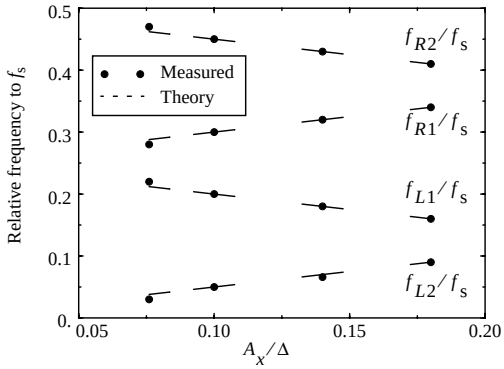

Fig. 9: Idle tones for an input tone at $f_s/4$ as a function of A_x/Δ.

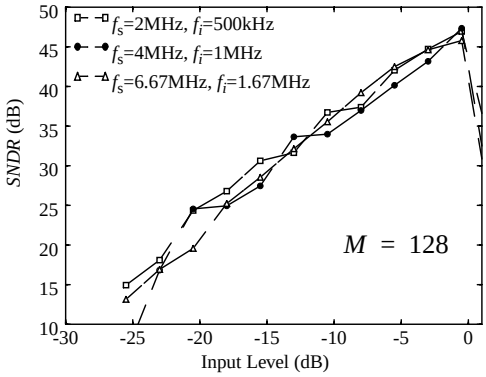

Fig. 10: Measured *SNDR* vs. input level for different AM frequencies when the input signal frequency is $f_s/4$.

In practical applications the input signal will contain spectral components at different frequencies, and according to (15), multiple tones will appear inside the signal band. This is verified by the following measurements.

B. Measurements for an input tone at f_n

Placing the input signal at the notch frequency of a BP-ΣΔM maximizes the dynamic range of such a modulator. However, for the case of a 2nd-order BP-ΣΔM, a large number of idle tones will appear, thus destroying the operation of the modulator. Fig.11 illustrates this by plotting a measured modulator output spectrum when clocked at $f_s = 2\text{MHz}$ corresponding to a single tone of -6dB input level and approximately located at the notch frequency.

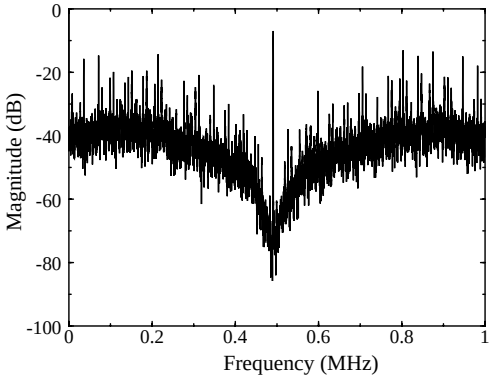

Fig. 11: Measured modulator output spectrum for a single tone at 491kHz of -6dB input level (2MHz sampling frequency).

According to (15), the frequency of idle tones only depends on the relative location of the input frequency with respect to $f_s/4$. However, as also shown in [8] for LP-ΣΔMs, the amplitude of such tones is strongly dependent on the input signal amplitude. Fig.12 illustrates this by plotting the central part of three measured output spectra corresponding to different input amplitudes. The position of some of the most significant tones are labelled. Observe that the amplitude of said tones is not an increasing function of the input level, in the same way as happens to LP-ΣΔMs [8].

The most critical idle tones are those appearing in the signal band because they degrade the linearity of the modulator. This is illustrated in Fig.13 by depicting the measured *SNDR* as a function of the input level. Note that a hard non-linear behaviour is obtained, thus destroying the modulator performance.

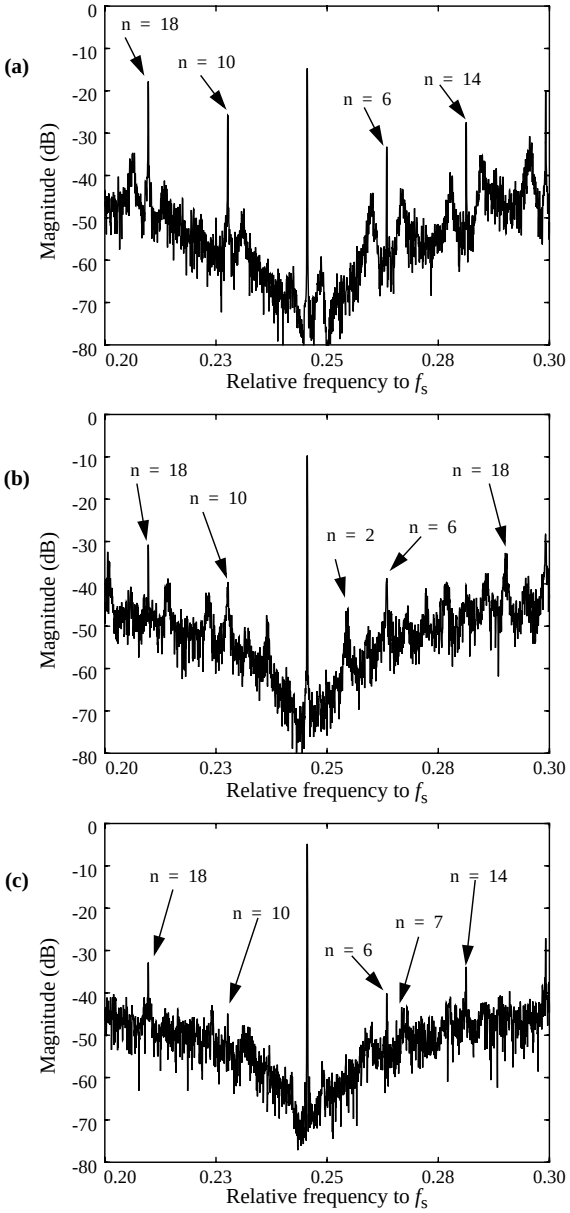

Fig. 12: Measured modulator output spectra for an input tone at $f_n = 0.2455 f_s$ ($\delta f_n = 0.0045 f_s$) and different input levels (a) –14.8dB , (b) –9.7dB and (c) –4.8dB .

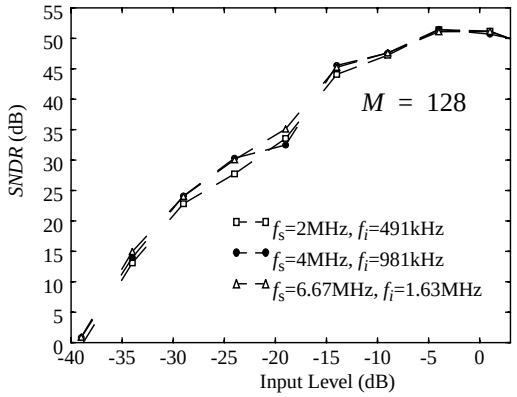

Fig. 13: Measured *SNDR* vs. input level for different AM frequencies for an input signal frequency at f_n .

Conclusions

This paper demonstrated experimentally the strong correlation between the quantization noise and the input signal in second-order bandpass ΣΔ modulators. This phenomenon has been studied considering either that the noise shaping is ideal or it is degraded by circuit parasitics. As a result of this study, close form expressions for the frequency of idle tones have been derived regarding different cases of the signal center frequency. All results have been validated by measurements from a 0.8μm CMOS prototype.

References

[1] R. Schreier and M. Snelgrove, "Bandpass Sigma-Delta Modulation", *Electronics Letters*, Vol. 25,pp. 1560-1561, November 1989.

[2] S.A. Jantzi, M. Snelgrove and P.F. Ferguson, "A Fourth-order Bandpass Sigma-Delta Modulator", *IEEE J. Solid-State Circuits*, Vol. 28, pp. 282-291, March 1993.

[3] F.W. Singor and W. M. Snelgrove, "Switched-Capacitor Bandpass Delta-Sigma A/D Modulation at 10.7 MHz", *IEEE J. Solid-State Circuits*, Vol. 30, pp. 184-192, March 1995.

[4] A.K. Ong and B.A. Wooley, "A Two-Path Bandpass ΣΔ Modulator for Digital IF Extraction at 20MHz", *IEEE Journal of Solid-State Circuits*, Vol. 32, pp. 1920-1933, December 1997.

[5] C.Toumazou, J.B.Hughes, and N.C. Battersby, *Switched-Currents: An Analogue Technique for digital technology*, London, Peter Peregrinus Ltd.,1993.

[6] J.M. de la Rosa, B. Pérez-Verdú, F. Medeiro and A. Rodríguez-Vázquez, "A 2.5MHz 55dB Switched-Current Band-Pass ΣΔ Modulator for AM Signal Conversion", *Proc. of the 1997 European Solid-State Cicuits Conference*, pp. 156-159, 1997.

[7] W. Bennett, "Spectra of Quantized Signals", Bell Syst. Tech. J., Vol. 27, pp.446-472, July 1948.

[8] R.M. Gray, "Quantization noise spectra", *IEEE Transactions on Information Theory*, Vol. 36, pp. 1220-1244, Nov. 1990.

[9] J.C. Candy and G.C. Temes: "*Oversampling Delta-Sigma Data Converters"*, IEEE Press, 1992.

[10] S.R. Norsworthy, R. Schreier, G.C. Temes: *"Delta-Sigma Converters. Theory, Design and Simulation"*, New York, IEEE Press, 1997.

[11] T. Y. Chang and S. R. Ribyk, "Exact Analysis of Second-Order Bandpass Delta-Sigma Modulator with Sinusoidal Inputs", *Proc. 1999 IEEE Int. Symp. Circuits and System*, Vol. 2, pp. 372-375, 1999.

[12] J.M. de la Rosa, B. Pérez-Verdú, F. Medeiro, R. del Rio and A. Rodríguez-Vázquez, "Non-Ideal Quantization Noise Shaping in Switched-Current Bandpass Sigma-Delta Modulators*", Proc. of 1999 International Symposium on Circuits and Systems*, Vol. 2, pp. 476-479, 1999.

[13] J.L. LaMay and H. T. Bogard, "How to Obtain Maximum Practical Performance from State-of-the-Art Delta-Sigma Analog-to-Digital Converters", *IEEE Trans. on Instrumentation and Measurement*, Vol. 41, pp. 861-867, December 1992.

[14] *MATLAB: User's Guide*, The MathWorks Inc., 1991.